EVALUATION OF FORCE-EQUILIBRIUM AND DEFORMATION-BASED DESIGN APPROACHES FOR PREDICTING REINFORCEMENT LOADS WITHIN GEOSYNTHETIC-REINFORCED SOIL STRUCTURES

Kuo-Hsin Yang [1], Panji Utomo [2], and Tai-Ling Liu [2]

ABSTRACT

The appropriate estimation of reinforcement loads is crucial for evaluating the internal stabilities of geosynthetic-reinforced soil (GRS) structures. The prediction methods used for the reinforcement loads within the GRS structures in the current research and practice can be categorized into two approaches: The force-equilibrium approach (*i.e.*, the earth pressure method and the limit equilibrium method) and the deformation-based approach (*i.e.*, the K-stiffness method and the finite element method). To date, the accuracy of these methods has not yet been examined and evaluated. In this paper, each method is introduced and their advantages and disadvantages are discussed. Afterward, the reinforcement loads measured from a 3.6 m high full-scale GRS structure using careful construction and instrumentation were used to examine the prediction of reinforcement loads using the aforementioned methods. The comparison results indicated that the force-equilibrium approach, including the earth pressure method and the limit equilibrium method, overestimates reinforcement loads up to 2.57 times. The finite element method is in good agreement with the measured data under working stress conditions; however, numerical illness (*i.e.*, the convergence problem) might occur earlier than the actual failure of the structure at large soil deformation (or strain) conditions. The K-stiffness method showed a clear underestimation in surcharging conditions. The reasons for the discrepancy between the predicted reinforcement loads and the measured data are discussed. The principal sources of the conservatism in the force-equilibrium approach to predict the reinforcement loads for the wall case used in this study are the inability to appropriately model the effect of facing, and the disregard for the strain compatibility between two dissimilar materials (*i.e.*, soil and reinforcement) in the force-equilibrium approach. The results obtained from this study provide insightful information for the design of GRS structures.

Key words: Geosynthetic-reinforced soil (GRS) structure, reinforcement load, force equilibrium, deformation.

1. INTRODUCTION

Mechanical stabilized earth (MSE) retaining structures are now widely used in various projects, including residences, highways, bridge abutments, and slope stabilization to increase the right of way (ROW), resist earth pressures, provide load bearing on top of MSE structures, and allow for changes of elevation in highway projects. Numerous factors have fostered the acceptance of MSE retaining structures. These include qualities such as pleasing aesthetics, reliability, and low cost. Moreover, appropriate construction techniques, impressive seismic performances, and a considerable ability to withstand sizeable deformations without structural distress account for the desirability of MSE structures. This study specifically focuses on the MSE retaining structures with extensible reinforcements, commonly called geosynthetic-reinforced soil (GRS) retaining structures. The three primary agencies identified in the most recent MSE structure design specifications in North America are the American Association of State Highway and Transportation Officials (AASHTO 2002, 2007), Federal Highway Administration (FHWA) (Elias *et al*. 2001; Berg *et al*. 2009), and National Concrete Masonry Association (NCMA 2010). In these design guidelines, the design of the MSE retaining structures is the result of a synergistic approach. Figure 1 shows that the wall system is analyzed for internal, external, global, and seismic stability, as well as deformability. The MSE structures must meet certain factors of safety, FS, against all failure models.

In analyzing the internal stability of the GRS structures, predicting the maximum reinforcement tensile load, T_{max}, in each reinforcement layer is required (Fig. 2). Knowing the forces in the reinforcements enables one to select reinforcements with adequate long-term strength (against breakage), to determine the length required to resist pullout within a stable soil zone (against pullout) and to calculate the required connection strength at the facing (against connection failure). As a result, the evaluation of T_{max} is critical for analyzing the internal stability of GRS structures. The prediction methods for the reinforcement loads within GRS structures in current research and practice can be

Manuscript received April 19, 2013; revised June 17, 2013; accepted June 20, 2013.

[1] Assistant Professor (corresponding author), Department of Construction Engineering, National Taiwan University of Science and Technology, 43, Sec. 4, Keelung Rd., Taipei, Taiwan (e-mail: khy@mail.ntust.edu.tw).

[2] Former Graduate Students, Department of Construction Engineering, National Taiwan University of Science and Technology, 43, Sec. 4, Keelung Rd., Taipei, Taiwan.

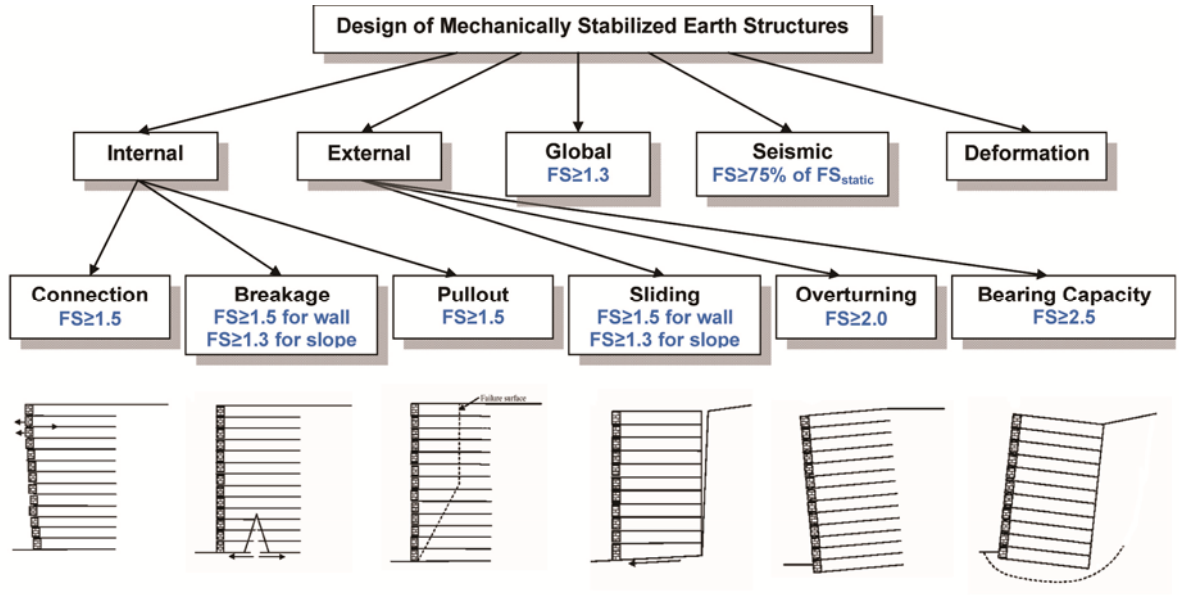

Fig. 1 Failure modes and safety factors for the design of MSE structures as required by FHWA (Elias *et al.* 2001; Berg *et al.* 2009)

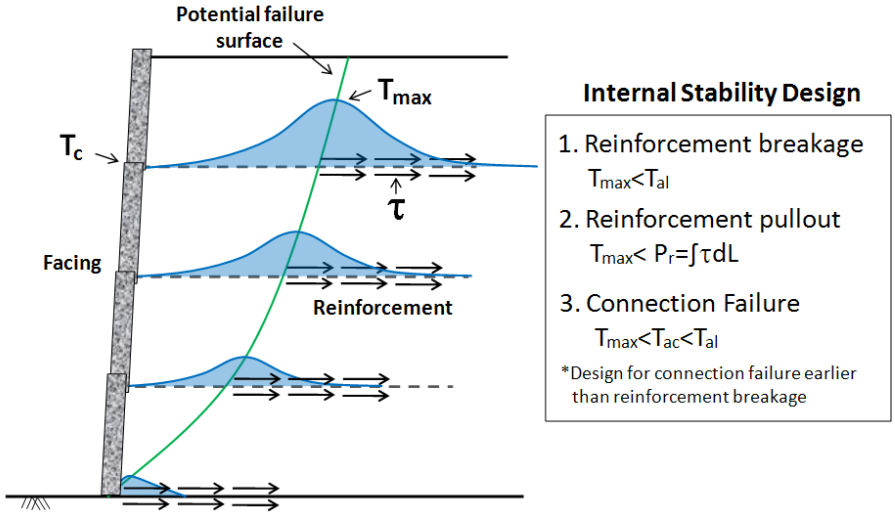

Fig. 2 Schematic illustration of reinforcement tensile loads mobilized within GRS structures and concept for internal stability analyses (T_{max} = maximum reinforcement tensile load; T_c = connection load; τ = soil-reinforcement interface shear stress: T_{al} = allowable reinforcement tensile strength; P_r = pullout capacity; T_{ac} = allowable connection strength)

categorized into two approaches: The force-equilibrium approach, namely, the earth pressure method and the limit equilibrium method, and deformation-based approach, namely, the K-stiffness method and the finite element method. The details of each method are discussed later.

Christopher *et al*. (2005) used a numerical model to illustrate the comparison of the earth pressure, limit equilibrium, and finite element methods. Their results indicate that the earth pressure theory overestimates the reinforcement loads in the GRS wall compared to the T_{max} predicted using the finite element method. Leshchinsky (2009) used a numerical benchmark test to examine the earth pressure and the K-stiffness methods. The benchmark test is based on a global static limit equilibrium analysis in which the sum of maximum reinforcement loads, ΣT_{max}, can be evaluated. Leshchinsky concluded that the earth pressure method might yield particularly conservative results for GRS structures with elevated facing stiffness (*i.e.*, concrete block facing). The K-stiffness method might violate statics, potentially leading to underestimating the reinforcement force. However, to date, the aforementioned prediction methods have yet not been assessed by comparing them with the measured T_{max} from physical walls.

Accordingly, the mentioned observation prompted this study to examine the effects of these methods on predicting the reinforcement tensile load T_{max} within GRS structures. In this paper, each method is first introduced and their advantages and disadvantages are discussed. The accuracy of each method is subsequently examined by comparing the predicted T_{max} with the measured T_{max} from a full-scale (3.6 m high) and carefully instrumented GRS wall. The reasons of the discrepancy between the predicted and the measured T_{max} are discussed at the end of this paper.

2. PREDICTION METHODS

2.1 Earth Pressure Method

The earth pressure method has been adopted in many current design guidelines (AASHTO 2002, 2007; Elias *et al*. 2001; Berg *et al*. 2009; NCMA 2010) to predict the reinforcement loads inside MSE walls. The design rationale assumes that the tensile forces developed in reinforcements are in local equilibrium with the lateral earth pressure generated in MSE walls. The FHWA design guidelines recommend using Eq. (1) to predict the T_{max} of each reinforcement layer:

$$T_{max} = \left(\frac{k_r}{K_a} \right) K_a (\gamma z + q) S_v \quad (1)$$

where T_{max} = maximum reinforcement load of each reinforcement layer; k_r / K_a = normalized lateral earth pressure coefficient; K_a = theoretical Rankine (adopted in AASHTO and FHWA) or Coulomb (adopted in NCMA considering both face inclination and soil-facing friction) active earth pressure coefficient; γ = backfill unit weight; z = depth below the top of the structure, q = surcharge, S_v = tributary area (equivalent to the reinforcement vertical spacing when analyses are carried out per unit length of wall). The k_r / K_a varies with the type of reinforcement; for flexible MSE or GRS walls, the k_r / K_a has a value of 1.0 and remains constant throughout the depth of the wall. This implies that, for flexible MSE or GRS walls, the horizontal movement occurring during construction is sufficient for the soil to reach an active stress state and generate an active earth pressure. The final computed reinforcement tensile loads increase linearly from the topmost layer to the bottommost layer of reinforcement (proportional to the overburden pressure).

Christopher *et al*. (2005) discussed the limitations of the earth pressure method as follows: (a) it is theoretically-based and, thus, it is limited to relatively simple geometric structures and difficult to extrapolate to complex geometries, such as narrow and multi-tiered walls; (b) it is limited to uniform granular soils and difficult to extrapolate to non-ideal reinforced fill soils; (c) the drainage should be adequate because pore water pressure or seepage forces in the reinforced fill are disregarded; (d) it cannot evaluate global stability; (e). the downdrag at connections is not evaluated; (f) it cannot be used to evaluate the wall deformation.

In addition, Allen *et al*. (2003) and Bathurst *et al*. (2008, 2005) investigated quantitatively the accuracy of reinforcement loads predicted using the earth pressure theory by carefully interpreting a database of 30 well-monitored, full-scale walls. By comparing the reinforcement loads (estimated from measured strains) in various instrumented GRS walls and the reinforcement loads predicted using earth pressure theory, they concluded that the loads predicted using earth pressure theory were excessively conservative. The predicted loads for the GRS walls were, on average, three times greater than the estimated values for the full-scale instrumented walls. Furthermore, the distribution of reinforcement loads in the instrumented walls was considered trapezoidal in shape rather than linear with depth, as assumed in the earth pressure theory for walls with uniform reinforcement spacing. Finally, Yang *et al*. (2012) observed from a series of finite element simulations that the mobilization of soil stress was non-uniform along the failure surface. This finding contradicts the basic assumption of the earth pressure method that the soil shear strength along the failure surface mobilizes equally and reaches the peak shear strength simultaneously. Overall, the earth pressure method produces safe structures, but is conservative regarding the reinforcement strength for MSE structures which are built on firm foundations and the reinforced fills that do not have positive pore water pressures.

2.2 Limit Equilibrium Method

The limit equilibrium (LE) method has been used to analyze the slope stability for years by assuming that the soil at failure obeys the perfectly plastic Mohr-Coulomb criterion and LE searches for a critical failure surface that contains a minimal factor of safety. The LE method can be applied to design problems with complex geometry (*e.g.*, multi-tiered structures) and non-homogeneous soils. It can include the effects of pore water pressure on system stability. The LE method can also evaluate global stability, as well as local stability, at any location or interface of interest. LE analyses of reinforced soil structures have also been reported (Zornberg *et al*. 1998; Yang *et al*. 2011). The stabilizing forces contributed by the reinforcement loads are incorporated into the equilibrium equation (balance of force or moment) at the "limit" state (exactly between stable and unstable states).

Christopher *et al*. (2005) discussed the limitations of design based on the LE method as follows: (a) the FHWA limits the use of the LE method to reinforced soil slopes (a facing inclination of less than 70°); however, this limitation is arbitrary and no theoretical reason exists for not extending it to reinforced walls (a facing inclination larger than 70°); (b) it requires modifications so that the connection load and the effect of the facing element can be assessed within the LE analysis; (c) the downdrag at connections is not evaluated; and (d) it cannot account for wall deformations.

The problem of the GRS structures in the LE analysis is statically indeterminate. In particular, the determination of T_{max} developed at each reinforcement layer requires assumptions. The validity of the assumption that the distribution of the reinforcement tensile loads with depth requires further verification. A triangular distribution of T_{max} (proportional to the overburden pressure) has been assumed in the design of reinforced soil structures (Schmertmann *et al*. 1987; Leschinsky and Boedeker 1989; Jewell 1991) (Fig. 3(a)). The FHWA design guidelines for reinforced soil slopes also recommend a linear distribution of T_{max} with depth by dividing T_{max} into two or three zones in the case of structures that exceed 6 m (Elias *et al*. 2001; Berg *et al*. 2009). However, as mentioned, the measured data show the nearly uniform mobilization of T_{max} with depth for the GRS walls under working stress and near failure conditions (Allen *et al*. 2003; Bathurst *et al*. 2008, 2005) (Fig. 3(b)). Regarding the GRS slopes, the conventional triangular distribution of T_{max} with depth is also unsupported by a centrifuge investigation that evaluated the behavior of reinforced soil slopes under working stress (Zornberg and Arriaga 2003) and failure (Zornberg *et al*. 1998) conditions. In their studies, the results of the analysis of the reinforcement strains show that the location of the maximum reinforcement strain among all the reinforcement layers does not occur near the toe of the structure. It was approximately located at the mid-height of the reinforced slopes, at a point along the critical failure surface and directly below the crest of the slope (Fig. 3(c)).

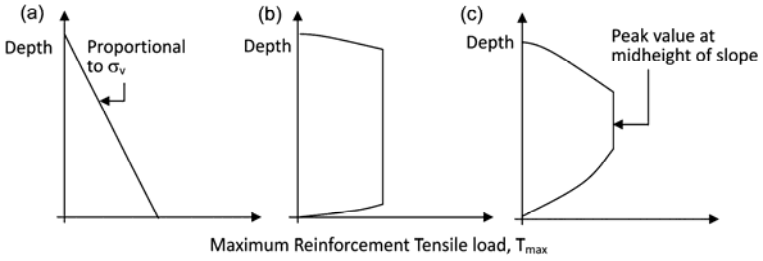

Fig. 3 Distributions of maximum reinforcement tensile loads with depth: (a) triangular distribution assumed in current design methods; (b) uniform shape for walls; (c) trapezoidal shape for slopes

2.3 K-Stiffness Method

Allen *et al*. (2003) and Bathurst *et al*. (2008, 2005) proposed an empirical method for estimating reinforcement loads in GRS walls under working stress conditions, known as the K-stiffness method. In the development of the K-stiffness method, a database of 30 wall case studies was used to establish an empirical expression for predicting T_{max} at each reinforcement layer. The K-stiffness method has altered the conventional equation, Eq. (1), for computing T_{max} by adding influence factors, Φ, calculated as

$$T_{\max} = \frac{1}{2} K_o (\gamma H + q) S_v D_{t\max} \Phi \tag{2}$$

$$\Phi = \Phi_g \, \Phi_{local} \, \Phi_{fs} \, \Phi_{fb} \, \Phi_c \tag{3}$$

where T_{max} = maximum reinforcement load; K_o = at-rest earth pressure coefficient; γ = backfill unit weight; H = wall height, q = surcharge; S_v = tributary area or the reinforcement vertical spacing; D_{tmax} = load distribution factor; Φ = influence factor, the product of factors that account for the effects of global and local reinforcement stiffness Φ_g and Φ_{local}, facing stiffness Φ_{fs}, face batter Φ_{fb}, and backfill cohesion Φ_c.

The limitations of design based on the K-stiffness method include the following: (a) the applicability of the K-stiffness method is limited to walls with a range of parameters matching the database of the case histories used to calibrate the K-stiffness method; (b) compared to earth pressure theory, the K-stiffness method involves numerous design variables and long design procedures; (c) the connection load is not included in the K-stiffness method; (d) this method is limited to relatively simple geometric structures; and (e) the pore water pressure in the reinforced fill is disregarded, which is implicitly assumed that soils are adequately compacted and that an appropriate drainage practice is exercised to keep water from entering the reinforced soil zone. In addition, the application of the K-stiffness method is limited to the GRS walls under working stress conditions. Allen *et al*. (2003) adequately predicted the T_{max} for GRS walls under working stress conditions (developed soil strain ≤ 3%). However, regarding GRS structures under large soil strain conditions (developed soil strain > 3%), the K-stiffness method consistently underestimated T_{max} because the K-stiffness method was developed based on T_{max} data from physical walls under serviceable conditions.

2.4 Finite Element Method

The finite element (FE) method has been widely applied to model the behavior of GRS structures (Yang *et al*. 2012; Hatami and Bathurst 2005, 2006; Ling *et al*. 2000; Karpurapu and Bathurst 1995; Lopes *et al*. 1994). An analysis based on the FE method accounts for full continuum mechanics, namely, the constitutive relationships of all of the materials involved. It satisfies the boundary conditions, accounts for local conditions such as the interface between soil and reinforcement, and can be applied to any loading condition and sequence, namely, traffic loading, seismic loading, and step loading, to simulate the construction sequence. Unlike the earth pressure and LE methods, its potential to produce displacements and compatibility between dissimilar materials is analytically assured. It can realistically represent a problem and its performance predictions can be accurate. It provides rich information concerning stress, strain, force, and displacement, and can be obtained at any location of interest (*e.g.*, at the nodal and Gaussian point).

Christopher *et al*. (2005) discussed the limitations of design based on the FE method as follows: (a) typically it requires a computational effort by a trained analyst; (b) it requires the comprehensive characterization of the strength and compressibility for all soils, reinforcements, and facings to produce relevant results; (c) it requires careful modeling to replicate the effects of soil-reinforcement-facing interactions; and (d) predictions can be non-conservative, requiring careful evaluation of the reliability of input values and the appropriate safety and resistance factors. In addition, although it has accurately predicted the behavior of GRS structures under working stress conditions, the FE method has not been reported to successfully predict under failure or sizeable deformation conditions. Numerical difficulties often occur under failure or large deformation conditions. This is a crucial problem for the evaluation of the structure behavior, specifically for comparatively flexible structures, such as GRS structures. Specific developments and implementations in this method are required for modeling the GRS structures under large deformation conditions. For example, a soil constitutive model is required to model the soil post-peak behavior. In addition, numerical accuracy and stability for simulations under large deformation conditions require particular care.

3. FULL-SCALE GRS WALL TEST

The mentioned methods to predict T_{max} are examined through a comparison of the T_{max} measured from a carefully instrumented full-scale GRS wall conducted by Bathurst *et al*. (2006) at Royal Military College (RMC). The GRS wall is 3.6 m high and constructed using six reinforcement layers at a spacing of S_v = 0.6 m. Unlike a typical wrapped-face GRS wall, in which each facing wrap is extended back into the reinforced soil zone, each facing wrap in this test wall was attached to the reinforcement layer above using a metal bar clamp to form the wall face with a facing slope of ω = 8°. Figure 4 illustrates the cross- section of the GRS test wall.

The backfill, named the RMC sand, is a clean, uniform graded, beach sand classified as poor sand according to the USCS. The backfill soil has D_{50} = 0.34 mm, a coefficient of curvature C_c = 2.25, a coefficient of uniformity C_u = 1.09, a unit weight γ = 16.7 kN/m^3, a soil peak friction angle ϕ_{tx} = 39°,

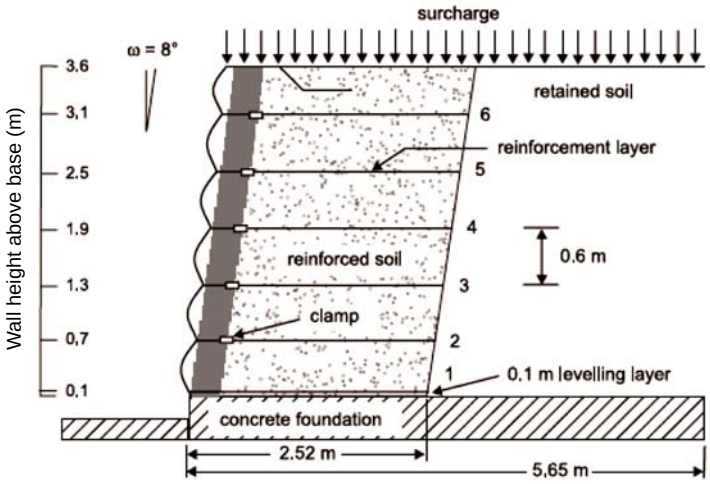

Fig. 4 Cross-section of the GRS test wall (Bathurst *et al.* 2006)

according to triaxial compression tests, and ϕ_{ps} = 42°, according to plane strain tests. The reinforcement was a polypropylene (PP) geogrid with a total length of 2.52 m, measured from the front wall face. The ultimate tensile strength was T_{ult} = 13 kN/m, which was obtained from a wide width strip tensile test (ASTM D4595). Because the reinforcement strain rate (10%/min) in the wide width tensile test is much higher than the strain rate that possibly developed in the test wall, a series of constant-load creep tests were carried out by Bathurst et al. (2006) to determine the isochronous load-strain responses of the reinforcement at 1,000 hr which approximates the duration of the wall test. The determined isochronous load-strain responses of the reinforcement at 1,000 hr was T_{ult} = 7.7 kN/m and the stiffness at 2% strain was $J_{2\%}$ = 100 kN/m.

The backfill was placed in 150 mm lifts matching the height of the facing units and compacted to the target density γ = 16.7 kN/m^3 with a 3% ~ 5% amount of moisture content. After completion of wall construction, uniform surcharges were applied on the top of the wall with load increments of 10 kPa until a final loading of 80 kPa was reached. The wall was intensively instrumented to measure its performance at the end of the construction and during the staged uniform surcharging; for instance, the strain gauges and extensometers attached to reinforcements were used to measure the reinforcement strains along each reinforcement layer. The measured maximum reinforcement strain at each reinforcement layer was then multiplied by the reinforcement secant stiffness ($T_{max} = J(\varepsilon) \times \varepsilon$), which was determined from the isochronous load-strain responses at the same strain level to estimate the reinforcement loads in this study.

4. CALCULATION DETAIL

4.1 Earth Pressure Method

Regarding the test wall without a backslope, the lateral earth pressure coefficient K_a in Eq. (1) can be calculated according to Rankine's and Coulomb's theories, as shown in Eqs. (4) and (5), respectively:

$$K_a = \tan^2\left(45 - \frac{\phi}{2}\right) \tag{4}$$

$$K_a = \frac{\cos^2(\omega + \phi)}{\cos^2\omega\cos(\delta - \omega)\left[1 + \sqrt{\dfrac{\sin(\phi + \delta)\sin\phi}{\cos(\delta - \omega)\cos\omega}}\right]^2} \tag{5}$$

where ϕ = backfill friction angle; ω = facing batter; δ = soil-facing interface friction angle. Unlike Rankine's theory, Coulomb's theory accounts for the effect of the wall facing batter and the soil-face interaction on K_a, resulting in the calculated K_a being less than the K_a from Rankine's theory. The peak plane strain friction angle of ϕ_{ps} = 42° was inputted into Eqs. (4) and (5) to characterize the backfill shear strength in the test wall conditions. In the calculation using Coulomb's theory, $\delta = \phi$ was used, assuming that the facing column creates a soil-to-soil interface for the wrapped-face wall. In this case, the difference in Coulomb's K_a between δ = 0° and $\delta = \phi$ was only 7%. The normalized lateral earth pressure coefficient of k_r / K_a = 1 was applied for the GRS test wall. The input values for other parameters in Eq. (1) corresponded to the physical wall test.

4.2 Limit Equilibrium Method

The limit equilibrium analyses were performed by applying the modified Bishop method with circular surfaces, as coded by the commercial slope stability analysis software, STEDwin. Figure 5 shows the LE modeling of the GRS test wall. The geometry of the wall model follows the dimensions of the physical wall test. The peak plane strain friction angle of ϕ_{ps} = 42° was used. The LE analysis assumed that the reinforcement forces had a uniform distribution through depth and accounted for the contribution of the geogrid overlap layers to the system's stability. Unlike the recommended use of the allowable tensile strength in the conventional analysis, the LE analyses in this study did not account for the reduction factors because of installation damage, creep, or degradation (*i.e.*, all the reduction factors were 1.0). A series of uniform loadings were applied on the top of the LE model to simulate the surcharges. The mobilized reinforcement loads T_{max} at different surcharges were determined by varying the values of T_{max} until FS = 1 was reached at each surcharge level.

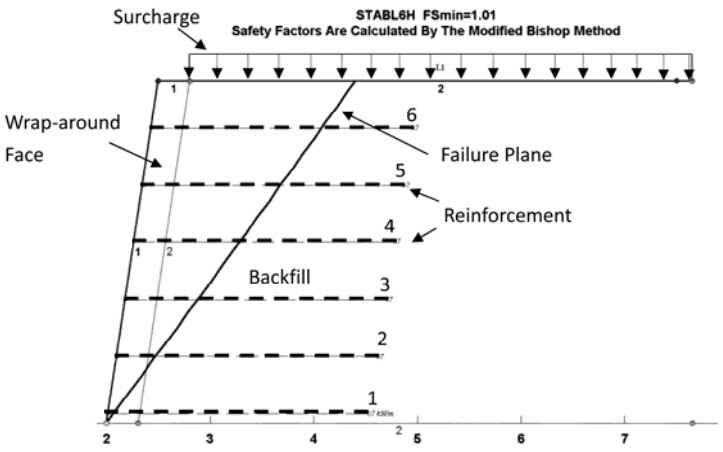

Fig. 5 Limit equilibrium model and results of the GRS test wall

4.3 K-Stiffness Method

As suggested by the K-stiffness method, the peak plane strain friction angle of $\phi_{ps} = 42°$ was used in the calculation. The reinforcement stiffness at 2% strain $J_{2\%} = 100$ kN/m, which was determined from the project-specific isochronous load-strain response was applied to calculate the influence factor for the effects of the global and local reinforcement stiffness (*i.e.*, Φ_g and Φ_{local}, respectively). The facing stiffness of $\Phi_{fs} = 1$ was applied according to the suggestion in the K-stiffness method. This implies that the wrapped-around face exerts no influence on the calculated T_{max}. Specifically, the wrapped-around face cannot reduce the reinforcement loads by resisting a part of the lateral earth pressure. Because the cohesion in the backfill is non-existent, the effect of the cohesion is not considered in the calculation (*i.e.*, $\Phi_c = 1$). The input values for other parameters in Eqs. (2) and (3) correspond to the physical wall test.

4.4 Finite Element Method

The FE program, PLAXIS version 8.2 (PLAXIS 2005), was used to develop a numerical model for the GRS test wall at the end of construction and during the staged uniform surcharging. Figure 6 shows the FE model of the GRS test wall. The backfill, the RMC sand, was modeled as a stress-dependent, hyperbolic elasto-plastic material using the Hardening Soil model. Table 1 lists the material properties of the RMC sand calibrated using plane strain and triaxial compression tests. The soil plane strain properties were selected for the FE simulation. Figure 7 shows the measured and predicted results of the stress-strain-volumetric response of the RMC sand. A small cohesion value, $c = 1$, and 2 kPa were introduced in the soil model during construction and during the staged uniform surcharging, respectively, to improve the numerical stability. In addition, because each facing wrap was fixed using a metal bar clamp in the test wall, a cohesion of $c = 10$ kPa was applied to the soil elements in the wrapped-around face to simulate this effect. The reinforcements were modeled as elasto-plastic bar elements with an axial stiffness EA, maximum axial tensile strength, N_p and no compressive strength. Table 1 lists the reinforcement properties determined from the isochronous load-strain response at 1,000 hr. Figure 8 shows the calibration results of the geogrid load-strain response. To model the nonlinear load-strain response, the reinforcement stiffness was inputted as $EA = 100$ kN/m and 70 kN/m for construction and during the staged uniform surcharging, respectively. These input values of reinforcement stiffness correspond to the average mobilized reinforcement strains of 2% and 7% during construction and during staged uniform surcharging, respectively.

The stage construction was included in the simulation by conducting layer-by-layer constructions in PLAXIS. The uniform surcharges were applied on the top of the FE model with load increments of 10 kPa until the target loading of 80 kPa was reached. The updated mesh and the arc-length control were activated to account for sizeable system deformations, which were particularly critical under substantial loading conditions. Notably, the calculated FE failure occurred earlier than the actual failure of the soil when a clear internal surface failure was observed in the test wall at $q = 90$ kPa. The FE simulation terminated at the next 10 kPa loading increment after completing 40 kPa because of numerical difficulties occurred in the computation. The FE

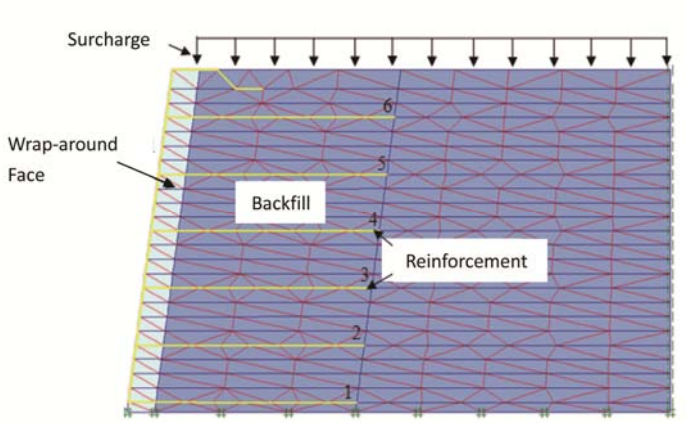

Fig. 6 Finite element model of the GRS test wall

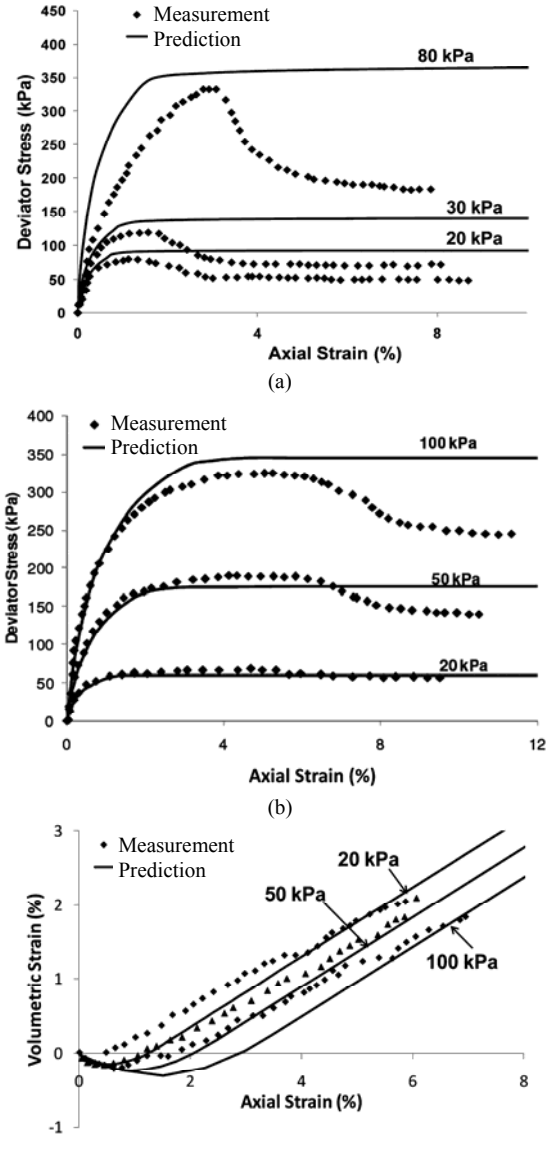

Fig. 7 Measured and predicted stress-strain-volumetric response of RMC sand: (a) stress-strain response from plane strain tests; (b) stress-strain response from triaxial tests; (c) axial strain-volumetric strain from triaxial tests (Note: No volumetric strain response was taken in plane strain tests.)

Table 1 Material properties for RMC sand and geogrid

Material	Value
Backfill	
γ (unit weight) (kN/m^3)	16.7
ϕ (friction angle) (degree)	42 (39)
c (cohesion) (kPa)	1 for construction 2 for surcharging 10 for wrapped-around face
ψ (dilation angle) (degree)	11
E_{50}^{ref} (secant stiffness) (kPa)	6.2×10^4 (2.76×10^4)
E_{oed}^{ref} (tangent stiffness for primary odeometer loading) (kPa)	6.0×10^4 (2.76×10^4)
E_{ur}^{ref} (unloading/reloading stiffness) (kPa)	1.8×10^5 (8.28×10^4)
m (modulus exponent)	0.5
R_f (failure ratio)	0.8
Reinforcement	
N_p (maximum tensile strength) (kN/m)	7.7
EA (axial stiffness) (kN/m)	100 for construction 70 for surcharging

Note: E_{ur}^{ref} was assumed to be $3E_{50}^{ref}$ as the default setting in PLAXIS; values in parenthesis are for simulation of soil behavior under triaxial compression in Fig 7.

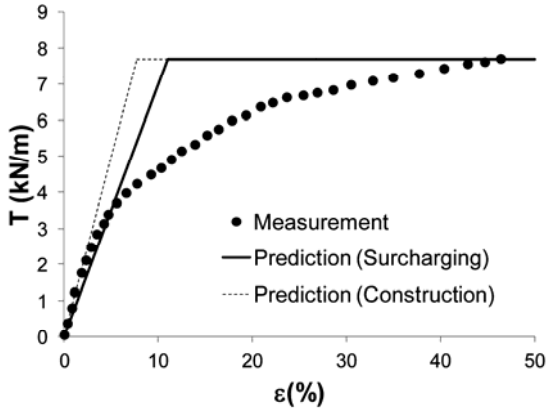

Fig. 8 Measured and predicted isochronous load-strain response of geogrid

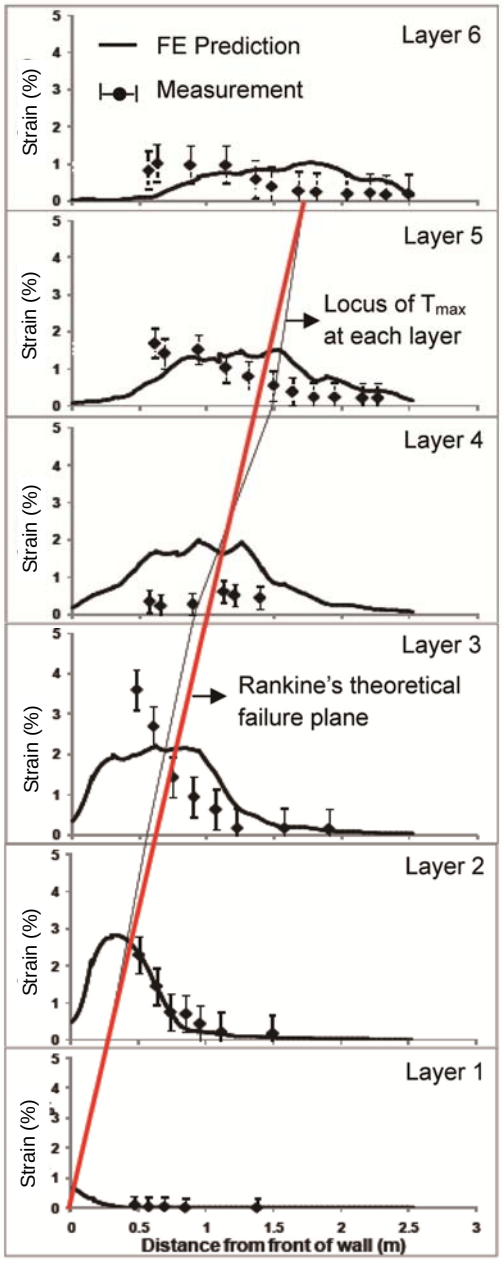

Fig. 9 Measured and predicted reinforcement strain along each reinforcement layer after construction (q = 0 kPa). The range bars represent 10% of uncertainties on measured strain.

output reveals that over 5% of the soil strain was mobilized along the failure surface at q = 40 kPa. Compared with the plane strain test results in Fig. 7, the mobilization of 5% of the soil strain indicated that the soil had already reached its peak strength at this loading stage. Figure 9 demonstrates the verification of the FE model by comparing the predicted and the measured reinforcement strains along each reinforcement layer at q = 0 kPa.

5. RESULTS AND DISCUSSION

5.1 Maximum Reinforcement Load T_{max}

The accuracy of each method is examined by comparing the predicted T_{max} with the measured T_{max} from the test wall. Figure 10 shows the comparison of T_{max} at q = 0 kPa (the end of construction), q = 40 kPa, and q = 80 kPa. The "measured" reinforcement load in Fig. 10 indicates the estimated reinforcement load calculated by multiplying the measured strain by using the isochronous stiffness value at the same strain level for each reinforcement layer. The error bars in Fig. 10 represent 10% of the uncertainties of the estimated T_{max} to account for the error of the strain measurements and the reinforcement stiffness interpretation. Because Bathurst *et al.* (2006) only reported the strain magnitude and distribution in the six layers of the reinforcements at q = 0 and 80 kPa, no measured T_{max} data at q = 40 kPa is shown in Fig. 10(b). In addition, the FE simulation in this study terminated at q = 40 kPa; therefore, no FE results can be shown in Fig. 10(c) for q = 80 kPa. Overall, the comparison results

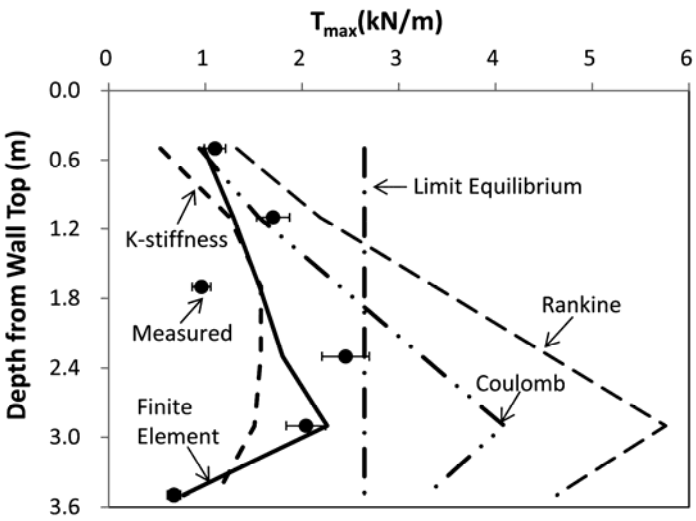

(a) q = 0 kPa (end of construction)

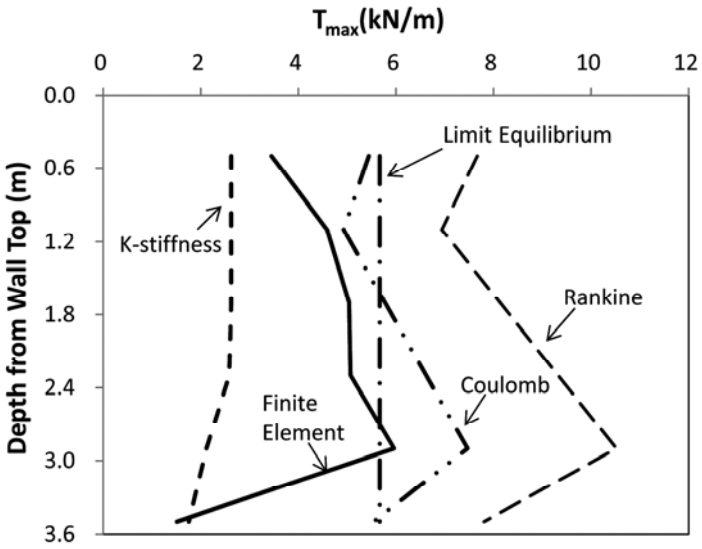

(b) q = 40 kPa

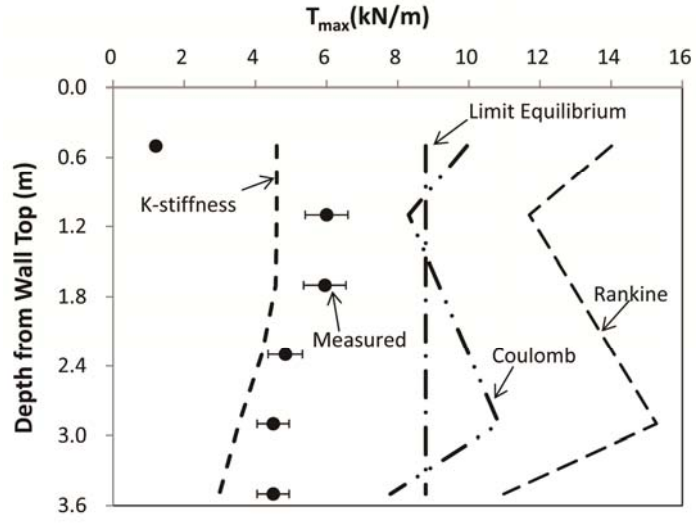

(c) q = 80 kPa

Fig. 10 Comparison of reinforcement load T_{max} at each reinforcement layer

indicate that the earth pressure methods using both Rankine's and Coulomb's theories overly predict the reinforcement loads. The earth pressure method using Coulomb's theory is considered superior to that using Rankine's theory because Coulomb's theory can account for the effect of the wall facing batter and the soil-face interaction on K, which predicts that T_{max} values are closer to the measured T_{max}. Although the T_{max} at q = 0 kPa predicted using the LE method is in good agreement with the maximum value of the measured T_{max}, the uniform distribution of the reinforcement load with the depth assumed in the LE method does not match the distribution of the measured data. The K-stiffness method seems to underestimate the measured T_{max} after construction (Fig. 10(a)) and at q = 80 kPa (Fig. 10(c)). The FE predictions agree substantially with the measured T_{max} in Fig. 10(a).

5.2 Maximum of Maximum Reinforcement Load T_{maxmax}

Figure 11 shows the comparison of the maximum of the T_{max} among all the reinforcement layers (*i.e.*, T_{maxmax}) at various surcharge levels. Predicting the T_{maxmax} value accurately is critical because this value is conventionally used to determine the reinforcement tensile strength in the internal design of the GRS wall against reinforcement breakage. The measured T_{maxmax} is obtained from reinforcement layer 3, the highest loaded reinforcement layer as mentioned in Bathurst *et al*. (2006). Overall, each method can predict the increase of the T_{maxmax} with increasing surcharges. However, except for an accurate prediction of T_{maxmax} at q = 0 kPa using the LE method, the force-equilibrium approach, including the earth pressure methods using Rankine's and Coulomb's theories and the LE method, overly predicts the reinforcement loads at various surcharge levels. The magnitude of the discrepancy between the predicted and the measured results increases as the surcharge increases.

Regarding the deformation-based approach, the K-stiffness method slightly underestimates the measured T_{maxmax} at q = 0 kPa; however, it displays an substantial underestimation under surcharging conditions. This observation is consistent with one of the K-stiffness method's limitations as discussed by Allen *et al*. (2003). The prediction of the FE method agrees well with the measured T_{maxmax}. As mentioned, the FE simulations terminated at the next 10 kPa loading increment after reaching 40 kPa because of the numerical difficulties that occurred in the computation. Therefore, the FE results are only presented until q = 40 kPa (Fig. 11). Table 2 summarizes the ratio of the predicted T_{maxmax} to the measured T_{maxmax} under various surcharge levels. The earth pressure method using Rankine's theory displays the most substantial overestimation of the T_{maxmax} value by an average ratio of 2.57. In contrast, the K-stiffness method underestimates the T_{maxmax} value most substantially with an average ratio of 0.64.

5.3 Sum of the Maximum Reinforcement Load $\sum T_{max}$

Figure 12 shows the comparison of the sum of T_{max} from all reinforcement layers (*i.e.*, $\sum T_{max}$) at various surcharge levels. As mentioned, because Bathurst *et al*. (2006) only reported the strain magnitude and distribution in the six layers of reinforcements at q = 0 and 80 kPa, only the measured $\sum T_{max}$ at q = 0 and 80 kPa are plotted in Fig. 12. Similarly to the previous observations in Fig. 11, the force-equilibrium approach overly predicts the mobi-

lized $\sum T_{max}$. The FE method agrees well with the measured data obtained under working stress conditions; however, numerical illness occurs under large soil deformation conditions ($q \leq$ 40 kPa). The K-stiffness method exhibits good agreement under working stress conditions (the end of construction), but underestimates the measured $\sum T_{max}$, in particular, under large loading conditions.

Leshchinsky (2009) performed a numerical benchmark test to examine whether the earth pressure and the K-stiffness methods satisfy the global static equilibrium in a limit state. Leshchinsky (2009, 2010) argued that although each design method yields a different T_{max} for each reinforcement layer, the ΣT_{max} over all the reinforcement layers predicted using any design approach requires meeting or exceeding the requirement for a global static equilibrium in the limit state. The benchmark test based on a static limit equilibrium analysis is shown in Fig. 13. The benchmark test is unsuitable for assessing the individual T_{max} value in each reinforcement layer. Only the sum of the reinforcement loads ΣT can be evaluated using the benchmark test. The closed-form solution for ΣT is

$$\Sigma T = \left(\frac{1}{2}\gamma H^2 + qH\right)\left(\frac{1}{\tan\theta} - \tan\omega\right)\tan(\theta - \phi) \qquad (6)$$

Table 2 Summary of ratio of predicted T_{maxmax} to measured T_{maxmax}

Methods	Surcharge level, q (kPa)								
	0	10	30	40	50	60	70	80	Average
Rankine	2.61	2.75	2.31	2.43	2.63	2.62	2.52	2.66	2.57
Coulomb	1.85	1.95	1.64	1.73	1.87	1.86	1.79	1.89	1.82
Limit equilibrium	1.11	1.23	1.16	1.27	1.42	1.42	1.42	1.50	1.32
K-stiffness	0.71	0.72	0.58	0.61	0.65	0.64	0.61	0.64	0.64
Finite element	1.02	1.08	1.09	1.16	N/A	N/A	N/A	N/A	1.09

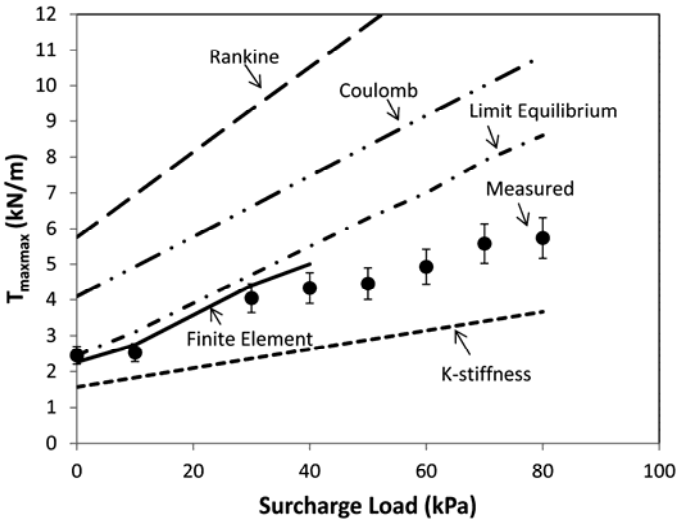

Fig. 11 Comparison of the maximum of maximum reinforcement load among all reinforcement layers T_{maxmax} at various surcharge levels

where γ = unit weight of backfill; q = surcharge; H = wall height; θ = inclination angle of failure plane; ω = face batter; ϕ = backfill friction angle. The calculation must be repeated for various θ until the maximum value of ΣT, $(\Sigma T)_{max}$, is determined. The benchmark test requires that the sum of the design values of T_{max} is equal to or exceeds the maximum of ΣT, which is required to maintain the global static equilibrium in the limit state (*i.e.*, $\Sigma T_{max,} \geq (\Sigma T)_{max}$). If $(\Sigma T)_{max} > \Sigma T_{max,,}$ the design approach underestimates the reactive force and the global static equilibrium is violated. Based on the results from the benchmark test, Leshchinsky concluded that the earth pressure method yields very conservative results for the GRS structures with elevated stiffness facing (*i.e.*, concrete block facing). The K-stiffness method violates statics, potentially leading to underestimation of the reinforcement force.

For the wall case used in this study, $(\Sigma T)_{max}$ was calculated using Eq. (6), which is also presented in Fig. 12 for comparison. One might observe that the $(\Sigma T)_{max}$ that is calculated using Eq. (6) almost overlaps on the line of the ΣT_{max} predicted by the earth pressure method using Coulomb's K_a because the fundamental

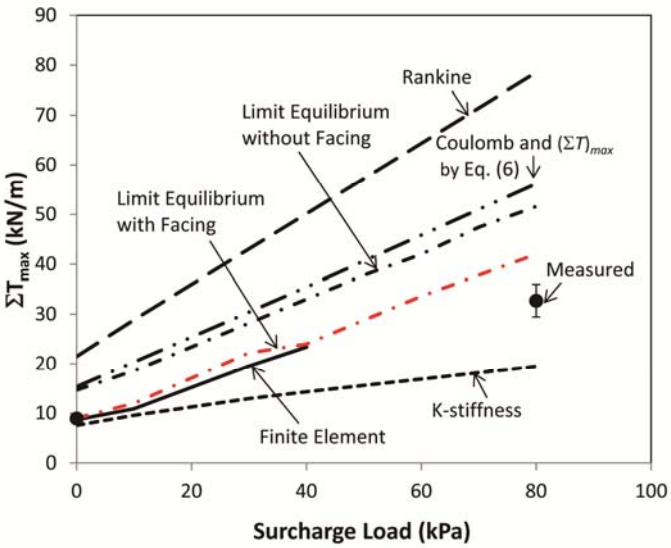

Fig. 12 Comparison of the sum of reinforcement loads from all reinforcement layers ΣT_{max} at various surcharge levels

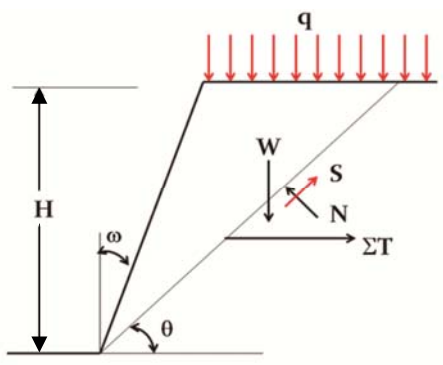

Fig. 13 Basic static limit equilibrium analysis for benchmark test by Leshchinsky (2009)

theories used to develop these two methods are identical: Both are based on the static equilibrium at the soil limit state. As reported by Leshchinsky (2009), $\Sigma T_{max,} > (\Sigma T)_{max}$ for the earth pressure method uses Rankine's K_a and $(\Sigma T)_{max} > \Sigma T_{max}$ for the K-stiffness method. Similarly to the K-stiffness method, the FE method produces $(\Sigma T)_{max} > \Sigma T_{max}$. In Leshchinsky's (2009) view, the FE method also violates the global static equilibrium. However, as discussed previously in Section 2.4, the computation in the FE method is governed by static equilibrium, compatibility, and the material constitutive law. Consequently, the global static equilibrium must be strictly obeyed in the FE calculation. In authors' opinion, using Eq. (6) to examine whether a prediction method satisfies or violates the global static equilibrium is arguable. Equation (6) can be viewed as one type of force-equilibrium approach, which is simply established on the equilibrium of static forces acting on a single sliding soil mass. The principal problem of using the force-equilibrium approach to predict T_{max} is discussed next.

6. DISCUSSION ON POSSIBLE SOURCES OF ERROR

In the 46th Karl Terzaghi lecture, Holtz (2010) discussed the discrepancy between the predicted and measured T_{max}, which might originate from the following:

(a) the selection of the soil shear strength properties to input into the prediction methods (*i.e.*, use of ϕ_{tx}, $\phi_{ps,}$ or $\phi_{residual}$);
(b) the influence of soil volumetric dilation;
(c) the error and uncertainty in estimating the reinforcement loads;
(e) the influence of facing stiffness.

These reasons have also been discussed by other researchers (Leshchinsky 2009, 2010; Bathurst *et al*. 2006). Additionally, the absence of consideration of the strain compatibility between two dissimilar materials (*i.e.*, soil and reinforcement) can be another critical source of error in the force-equilibrium approach. All of these issues are discussed in detail as follows.

6.1 Selection of the Soil Shear Strength Properties

To select the soil shear strength properties, the peak plane strain friction angle ϕ_{ps} was used in this study to characterize the backfill shear strength in the test walls because the test wall conditions conformed to the plane strain conditions. If other soil friction angle values (*i.e.*, ϕ_{tx} or $\phi_{residual}$ in which $\phi_{ps} > \phi_{tx} > \phi_{residual}$) are used in the calculation, the predicted T_{max} would be higher than that which is calculated using $\phi_{ps,}$ leading to further over-prediction, particularly in the force-equilibrium approach (Fig. 14). Bathurst *et al*. (2006) addressed a similar trend of T_{max}, which was calculated using three soil friction angle values for the backfill soil.

6.2 Influence of Soil Volumetric Dilation

The influence of soil volumetric dilation has been evaluated by Karpurapu and Bathurst (1995) by using FE simulations. They observed that the FE analyses with a backfill dilation angle ψ = 0° predicted much greater facing displacements and larger reinforcement strains compared to those with ψ = 15°. In certain cases, the over-prediction was greater than the measured values by a factor of two. In addition, by inputting the correct dilation angle (*i.e.*, ψ = 15°), the predicted ultimate loading and lateral facing displacement profile are closer to those observed in the physical experiment. Figure 15 shows the effect of soil volumetric dilation on the predicted T_{max} using the FE model in this study. The numerical results in Fig. 15 agree with the finding by Karpurapu and Bathurst (1995). Overall, the soil dilation can enhance the system stiffness and, hence, reduce the system deformation, resulting in less reinforcement strain and load mobilization. However, the influence of soil dilation is not accounted for in the force-equilibrium approach, leading to the over-prediction of T_{max}, as demonstrated in this study.

6.3 Error and Uncertainty in the Estimation of the Reinforcement Load

Loads in reinforcement layers are inferred from the strain measurements made using strain gauges or pairs of extensometers attached to the reinforcement layers. Bathurst *et al*. (2005, 2006) discussed that the error and uncertainly in estimating the loads in reinforcement layers originate from the strain measurement and reinforcement stiffness interpretation of in-isolation creep data. Based on the data for an instrumented PP geogrid, Bathurst *et al*. (2002) reported that strain gauges accurately estimated the reinforcement strains in a 0.02% ~ 2% range and that

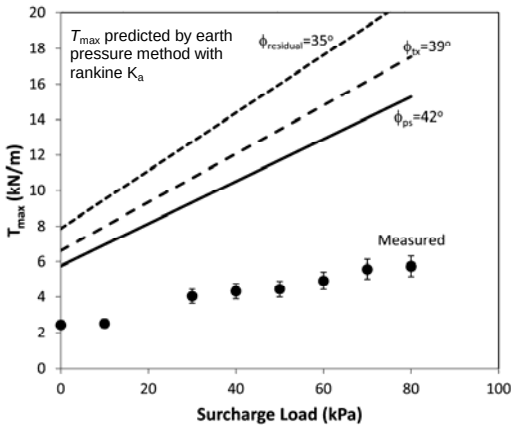

Fig. 14 Influence of soil shear strength on the predicted T_{max} by earth pressure method at various surcharge levels

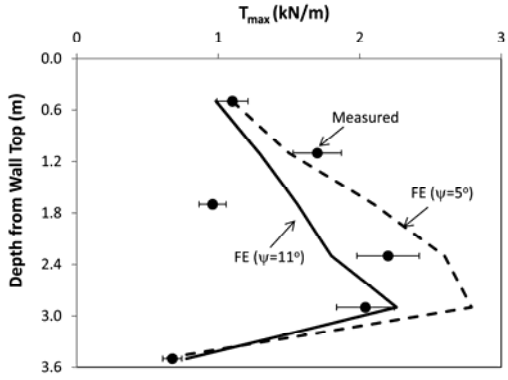

Fig. 15 Influence of soil volumetric dilation on the predicted T_{max} at end of construction (q = 0 kPa)

extensometers are more reliable for reinforcement strains ≥ 2%. They also calculated that the coefficient of the variation for the strain gauge readings (COV_ε) is 13% for a reinforcement strain of 0.02% ~ 2% and the COV_ε for the extensometer readings is 9% if the devices are restricted to strains ≥ 2%. Based on data presented in the investigation by Walters *et al*. (2002), the upper limit of the variation coefficient of the reinforcement stiffness value (COV_J) for the PP geogrid was calculated to vary between 5% and 13%. Uncertainties in the strain measurements (COV_ε) and the stiffness values (COV_J) are independent; therefore, the total uncertainty (COV_T) in the estimate of reinforcement loads can be calculated as follows:

$$COV_T = \sqrt{COV_\varepsilon^2 + COV_J^2} \tag{7}$$

Equation (7) is used to calculate the error bar in the plots for estimated reinforcement load values presented in this paper. Consequently, the error bars representing 10% of the uncertainties of the estimated T_{max} were determined to account for the error of the strain measurements and the reinforcement stiffness interpretation. Additionally, other variations in construction and environmental degradation, which could be the case for the field structures, were not considered in this study because the test wall was carefully constructed in an appropriately controlled environment in the RMC laboratory.

6.4 Existence of Apparent Cohesion

Leshchinsky (2009, 2010) used a sand castle as an example to declare that a trace of the apparent cohesion from the capillary suction or soil matrix potential in unsaturated field conditions might dramatically increase the systemic stability and result in reducing the requirements of T_{max} for equilibrium within the GRS structures. The effect of apparent cohesion might be critical for the field structures which might contain a substantial percentage of fines in the backfill soil. However, the influence that this effect exerts on the measured T_{max} for the test walls discussed in this study is insignificant because the backfill used in the test wall consisted of uniform beach sand with relatively coarse sand particles (*i.e.*, D_{50} = 0.34 mm) and of less than 1% fine soil. The backfill was compacted using 3% ~ 5% moisture content. The apparent cohesion in this backfill condition is likely to be minimal. To confirm this, three unconfined compression tests were conducted to measure the magnitude of the apparent cohesion of the Fulung sand specimens (Fig. 16). The Fulung sand has a particle distribution and shear strength properties similar to the RMC sand used in the test walls (Table 3 and Fig. 17). The Fulung sand specimens were prepared to the water content and relative density that approximated the compaction conditions in the test walls. The rationale lies in the unsaturated soil shear strength equation proposed by Fredlund *et al.* (1978):

$$\tau = c' + (\sigma - u_a)\tan\phi' + (u_a - u_w)\tan\phi^b \tag{8}$$

where τ = unsaturated soil shear strength; c' = effective cohesion of saturated soil; ϕ' = effective friction angle of saturated soil; σ = total stress on the failure plane; u_a = pore air pressure; u_w = pore water pressure; ϕ^b = angle indicating the rate of increase in shear strength relative to the matric suction. Additionally, $(\sigma - u_a)$ can be viewed as the net normal stress on the failure plane and $(u_a - u_w)$ is known as matric suction. Because the saturated sand does not have any shear strength under unconfined condition (*i.e.*, c' = 0 kPa and $\sigma - u_a$ = 0 kPa), the soil shear strength is measured using the unconfined compression test that can be attributed to the apparent cohesion c_a because of the effect of the soil suction, as shown by

$$c_a = (u_a - u_w)\tan\phi^b \tag{9}$$

The average unconfined compression strength measured from the Fulung sand specimens under the previously described test condition is approximately 3 kPa, suggesting that the apparent cohesion of the sand specimen has extremely limited value, which is approximately c_a = 1.5 kPa. This c_a value is further inputted into the LE program as the backfill cohesion to evaluate the influence of the apparent cohesion on the predicted $T_{max.}$ As shown in Fig. 18, when c_a = 1.5 kPa, the ratio of ΣT_{max} considering the apparent cohesion to ΣT_{max} without considering the

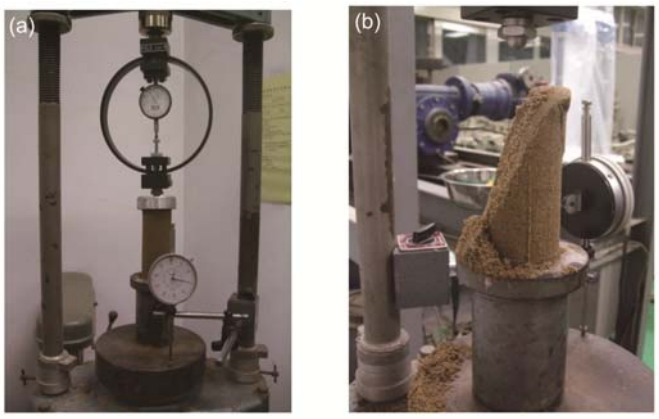

Fig. 16 Unconfined compression test to quantify the apparent cohesion of an unsaturated Fulung sand specimen: (a) before test; (b) failure of soil specimen

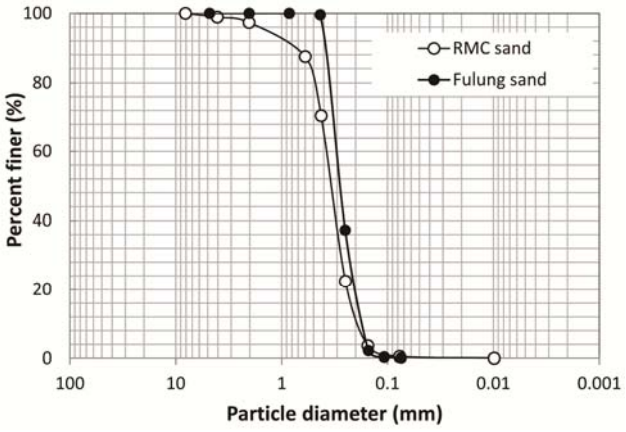

Fig. 17 Comparison of grain size distributions between RMC and Fulung sand

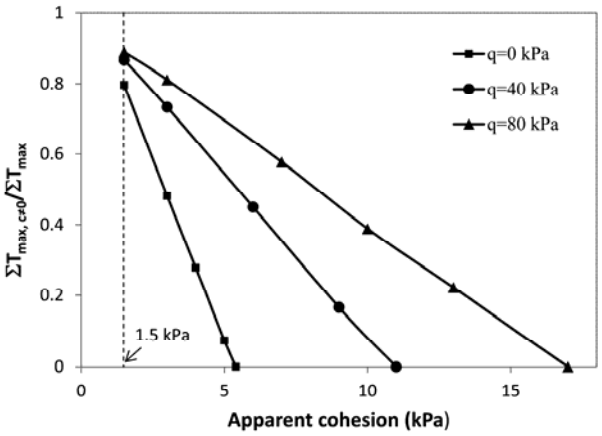

Fig. 18 Influence of apparent cohesion on predicted ΣT_{max} at different surcharge levels

Table 3 Comparison of material properties between RMC and Fulung sand

Soil	Origin	γ (kN/m^3)	ϕ_{tx} (degree)	D_{50} (mm)	C_c	C_u	USCS
RMC	Beach sand	16.7	39	0.34	2.25	1.09	SP
Fulung	Beach sand	15	39	0.28	0.95	1.76	SP

apparent cohesion (*i.e.*, $\Sigma T_{max,c\neq0} / \Sigma T_{max}$) ranges between 80% ~ 90%, which means a 10% ~ 20% reduction of ΣT_{max}, which occurs as q increases. The ratio of $\Sigma T_{max,c\neq0} / \Sigma T_{max}$ reaches zero (no reinforcement is required) when c_a = 5.4, 11 and 17 kPa at q = 0, 40 and 80 kPa, respectively. Finally, it should be reminded that the effect of the apparent cohesion due to the soil suction is typically not considered in the prediction of T_{max} because the design of the GRS structures should not rely on the soil shear strength, which might decrease or even disappear as the soil moisture increases.

6.5 Influence of the Facing Stiffness

Bathurst *et al*. (2006) mentioned that facing stiffness is one of the principal sources of conservatism in the force-equilibrium approach to predict T_{max}. They compared the influence of facing stiffness on the measured reinforcement strain and commented that the wall facing is a structural element that acts to reduce the magnitude of the deformation, resulting in reducing the reinforcement strain (or load) of the GRS structures. However, the influence of the facing stiffness is typically not accounted for in the current design procedures, which are established based on the force-equilibrium approach. In this study, the LE analyses were conducted by inputting an additional cohesion of c = 10 kPa to the soil elements in the wrapped-around face to simulate the effect of the facing stiffness. This method of modeling the facing stiffness is similar to the FE modeling discussed in Section 4.4. Again, unlike a typical wrapped-face GRS wall, in which each facing wrap was extended back into the reinforced soil zone, each facing wrap in the selected test wall was attached to the reinforcement layer above using a metal bar clamp to form the wall face. Hence, the use of clamps is likely to provide additional support to the facing.

The results of the LE analyses that account for the effect of the facing on the predicted ΣT_{max} are shown in Fig. 12. The LE results agree with the measured ΣT_{max} and the ΣT_{max} predicted using the FE method, which demonstrates that the modeling of the facing in the LE analyses can improve the prediction of the reinforcement loads. Some discrepancies between predictions and measurements, which can still be observed in Fig. 12, occur because the effect of facing cannot be easily and quantitatively implemented in the force-equilibrium method. More specifically, the resistance from facing should develop gradually with increasing loadings (*i.e.*, the increasing mobilization of the toe load or the connection load as the surcharge increases) rather than the constant value of cohesion assumed in this study. Further studies are required to more accurately simulate the effects of facing in the force-equilibrium approach.

6.6 Strain Compatibility

Yang *et al*. (2010) used stress data from a numerical study of a centrifuge model slope and two physical full-scale instrumented GRS retaining walls to examine the relationship between mobilized reinforcement load capacity and mobilized soil shear strength. The results indicate that the mobilization of the reinforcement tensile load capacity does not increase linearly with the mobilized soil shear strength until it reaches soil failure. Rather, the reinforcement tensile load increases slowly to approximately 10% of its ultimate tensile strength until the average mobilized soil shear strength along the failure surface reaches approximately 95% of its peak value. Even after the soil reaches a post-peak shear strength state, the reinforcement retained an additional 30% of its original tensile load capacity.

The results obtained from their study help to explain the observation that measured reinforcement loads in GRS walls in operational conditions are considerably lower than the predicted values using current force-equilibrium-based design methods. The force-equilibrium approach simply assumes that the tensile loads developed in reinforcement layers are in local equilibrium with the active lateral earth pressures generated in GRS structures. However, this assumption is based purely on force-equilibrium approach, which disregards the strain compatibility between two dissimilar materials (*e.g.*, soil and reinforcement). For example, as the system deformation increases, the force-equilibrium approach predicts that the mobilization of the reinforcement loads decreases with the change of the lateral soil earth pressure from an at-rest K_o to active K_a condition. In fact, the soil, the reinforcement strain, and the reinforcement load are mobilized because of the internal deformation of the GRS structures. Hence, the mobilization of the reinforcement load should increase as the system deformation increases. Moreover, the mobilized reinforcement tensile load in GRS structures are a function of the type of elongation and stiffness of the geosynthetic layers as they interact with and potentially influence and improve the confining soils. Consequently, design methodologies based on force-equilibrium cannot be expected to predict reinforcement loads accurately. The displacement-based analysis and design methods hold promise as alternative approaches for the selection of reinforcement materials and for the internal stability analysis of GRS structures.

7. CONCLUSIONS

In this paper, the accuracy of various design methods to predict the maximum reinforcement loads T_{max} was evaluated by

comparing with the measured data from a full-scale and carefully instrumented GRS structure. Specific critical conclusions and discussion points are summarized as follows:

- The comparison results indicate that the force-equilibrium approach, including the earth pressure and LE methods, overly predict reinforcement loads. Among all methods, the earth pressure method using Rankine's theory has the most substantial overestimate of the T_{max} value, which has an average ratio of 2.57.
- The FE method agrees well with the measured data under working stress conditions; however, numerical illness might occur earlier than the actual failure of the structures in large soil deformation conditions.
- The K-stiffness method slightly underestimated reinforcement loads under the working stress conditions (at the end of construction), but substantially underestimates reinforcement loads under the large loading conditions. Among all methods, the K-stiffness method underestimates the T_{max} value most substantially with an average ratio of 0.64.
- The force-equilibrium approach does not account for the strain compatibility between two dissimilar materials (*e.g.*, soil and reinforcement). The mobilization of the reinforcement strain and load are driven by systemic deformation. Consequently, the design methodologies based on the force-equilibrium approach cannot predict reinforcement loads accurately.
- The facing stiffness can reduce the system deformation and, consequently, reduce the reinforcement loads. This study demonstrated that the modeling of facing stiffenss in the LE anlaysis can improve the prediction of T_{max}. However, becasue the resistance from the facing should develop as the loading gradually increases, the effect of the facing cannot be easily and quantitatively implemented in the force-equilibrium method.

Finally, the prediction methods discussed in this paper are compared with the T_{max} obtained from one physical wall. The comparison results (*i.e.*, the ratio of predicted T_{max} to the measured T_{max} in Table 2) might vary with other wall and site cases. Despite the possible variations in other cases, the general trend, as discussed in this paper, remains valid and offers useful and insightful information for the design of GRS structures.

ACKNOWLEDGEMENTS

The financial support for this study was provided by the National Science Council of the Republic of China, Taiwan under Grant No. NSC99-2218-E-001-006 and partially by the National Taiwan University of Science and Technology under the new faculty member research funding.

NOTATIONS

The following symbols are used in this paper. Basic SI units are given in parentheses.

c	backfill cohesion	(N/m^2)
c_a	apparent cohesion for sand	(N/m^2)
C_c	coefficient of curvature	(dimensionless)
C_u	coefficient of uniformity	(dimensionless)
COV_ε	coefficient of variation of strain measurement	(dimensionless)
COV_J	coefficient of variation of reinforcement stiffness	(dimensionless)
COV_T	total coefficient of variation reinforcement load	(dimensionless)
D_{50}	median soil particle diameter	(m)
D_{tmax}	load distribution factor in K-stiffness method	(dimensionless)
E_{50}^{ref}	secant stiffness in FE model	(N/m^2)
E_{oed}^{ref}	primary consolidation stiffness in FE model	(N/m^2)
E_{ur}^{ref}	unloading/reloading stiffness in FE model	(N/m^2)
EA	axial stiffness of bar element in FE model	(N/m)
FS	factor of safety	(dimensionless)
H	wall height	(m)
$J_{2\%}$	reinforcement stiffness at 2% strain	(N/m)
k_r / K_a	normalized lateral earth pressure coefficient	(dimensionless)
K_a	active earth pressure coefficient	(dimensionless)
K_o	at-rest earth pressure coefficient	(dimensionless)
m	modulus exponent in FE model	(dimensionless)
N	normal force on failure plane	(N)
N_p	maximum axial tensile strength in FE model	(N/m)
P_r	pullout capacity	(N/m)
q	surcharge	(N/m^2)
R_f	failure ratio in FE model	(dimensionless)
S	shear force along failure plane	(N)
S_v	reinforcement vertical spacing	(m)
T	mobilized tensile load of reinforcement	(N/m)
T_{ac}	allowable connection load	(N/m)
T_{al}	allowable reinforcement tensile strength	(N/m)
T_c	connection load	(N/m)
T_{max}	maximum tensile load in a reinforcement layer	(N/m)
T_{maxmax}	maximum of T_{max} among all reinforcement layers	(N/m)
ΣT	sum of reinforcement loads	(N/m)
$(\Sigma T)_{max}$	maximum of sum of reinforcement loads	(N/m)
ΣT_{max}	sum of T_{max} from all reinforcement layers	(N/m)
$T_{max,c\neq 0}$	ΣT_{max} considering the effect of apparent cohesion	(N/m)
T_{ult}	ultimate reinforcement tensile strength	(N/m)
u_a	pore air pressure	(N/m^2)
u_w	pore water pressure	(N/m^2)
W	weight of soil failure wedge	(N)
z	depth below the top of the structure	(m)
δ	soil-facing interface friction angle	(degree)
ε	reinforcement strain	(dimensionless)
ϕ^b	soil shear strength angle relative to matric suction	(degree)
ϕ_{ps}	friction angle under plane strain condition	(degree)
ϕ_{tx}	friction angle under triaxial compression condition	(degree)
$\phi_{residual}$	residual friction angle	(degree)
Φ_c	backfill cohesion factor in K-stiffness method	

		(dimensionless)
Φ_{fb}	face batter factor in K-stiffness method	(dimensionless)
Φ_{fs}	facing stiffness factor in K-stiffness method	(dimensionless)
Φ_g	global reinforcement stiffness factor in K-stiffness method	(dimensionless)
Φ_{local}	local reinforcement stiffness factor in K-stiffness method	(dimensionless)
γ	backfill unit weight	(N/m^3)
θ	inclination of failure plane	(degree)
σ	normal stress	(N/m^2)
σ_v	overburden pressure	(N/m^2)
τ	shear stress/strength	(N/m^2)
ω	wall facing batter	(degree)
ψ	dilation angle in FE model	(degree)

REFERENCES

AASHTO (2007). *LRFD Bridge Design Specifications*. American Association of State Highway and Transportation Officials, 4th Ed., Washington, DC, USA.

AASHTO (2002). *Standard Specifications for Highway Bridges*. American Association of State Highway and Transportation Officials, 17th Ed., Washington, DC, USA.

Allen, T. M., Bathurst, R. J., Holtz, R. D., Walters, D., and Lee, W. F. (2003). "A new working stress method for prediction of reinforcement loads in geosynthetic walls." *Canadian Geotechnical Journal*, **40**(5), 976–994.

ASTM D4595. "Standard test method for tensile properties of geotextiles by the wide-width strip method." *The American Society for Testing and Materials*. West Conshohoken, PA.

Bathurst, R. J., Miyata, Y., Nernheim, A., and Allen, T. M. (2008). "Refinement of K-stiffness method for geosynthetic reinforced soil walls." *Geosynthetics International*, **15**(4), 269–295.

Bathurst, R. J., Vlachopoulos N., Walters, D. L., Burgess, P. G., and Allen, T. M. (2006). "The influence of facing stiffness on the performance of two geosynthetic reinforced soil retaining walls." *Canadian Geotechnical Journal*, **43**(12), 1225–1237.

Bathurst, R. J., Allen, T. M., and Walters, D. L. (2005). "Reinforcement loads in geosynthetic walls and the case for a new working stress design method." *Geotextiles and Geomembranes*, **23**(4), 287–322.

Bathurst, R. J., Allen, T. M., and Walters, D. L. (2002). "Short-term strain and deformation behavior of geosynthetic walls at working stress conditions." *Geotextiles International*, **3**(2), 205–225.

Berg, R., Christopher, B. R., and Samtani, N. (2009). *Design of Mechanically Stabilized Earth Walls and Reinforced Soil Slopes*. Vol. I and II, Report No. FHWA-NHI-10-024, National Highway Institute, Federal Highway Administration, Washington, D.C. U.S.A.

Christopher, B., Leshchinsky, D., and Stulgis, R. (2005). *Geosynthetic-Reinforced Soil Walls and Slopes: US Perspective*, *International Perspectives on Soil Reinforcement Applications.* ASCE Geotechnical Special Publication No. 141, ASCE Press, Reston, Virginia.

Elias, V., Christopher, B. R., and Berg, R. R. (2001). *Mechanically Stabilized Earth Walls and Reinforced Soil Slopes Design and Construction Guidelines*. Report No. FHWA-NHI-00-043, National Highway Institute, Federal Highway Administration, Washington, D.C. U.S.A.

Fredlund, D. G., Morgenstern, N. R., and Widger, R. A. (1978). "The shear strength of unsaturated soils." *Canadian Geotechnical Journal*, **15**(3), 313–321.

Hatami, K. and Bathurst, R. J. (2006). "Numerical model for reinforced soil segmental walls under surcharge loading." *Canadian Geotechnical Journal*, **67**(4), 1066–1085.

Hatami, K. and Bathurst, R. J. (2005). "Development and verification of a numerical model for the analysis of geosynthetic-reinforced soil segmental walls under working stress conditions." *Journal of Geotechnical and Geoenvironmental Engineering*, ASCE, **132**(6), 673–684.

Holtz, R. D. (2010). "Reinforced soil technology: From experimental to the familiar." *46th Karl Terzaghi Lecture, Geo- Institute of American Society of Civil Engineers*, *GeoFlorida Conference*, West Palm Beach, Florida.

Jewell, R. A. (1991). "Application of revised design charts for steep reinforced slopes." *Geotextiles and Geomembranes*, **10**(3), 203–233.

Karpurapu, R. G. and Bathurst, R. J. (1995). "Behaviour of geosynthetic reinforced soil retaining walls using the finite element method." *Computers and Geotechnics*, **17**(3), 279–299.

Leshchinsky, D. (2010). "Geosynthetic reinforced walls and steep slopes: Is it magic?" *Geosynthetics Magazine*, **28**(3), 16–24.

Leshchinsky, D. (2009). "On global equilibrium in design of geosynthetic reinforced wall." *Journal of Geotechnical and Geoenvironmental Engineering*, ASCE, **135**(3), 309–315.

Leshchinsky, D. and Boedeker, R. H. (1989). "Geosynthetic reinforced soil structures." *Journal of Geotechnical Engineering*, ASCE, **115**(10), 1459–1478.

Ling, H. I., Cardany, C. P., Sun, L.-X., and Hashimoto, H. (2000). "Finite element study of a geosynthetic-reinforced soil retaining wall with concrete-block facing." *Geosynthetics International*, **7**(3), 163–188.

Lopes, M. L., Cardoso, A. S., and Yeo, K. C. (1994). "Modelling performance of a sloped reinforced soil wall using creep function." *Geotextiles and Geomembranes*, **13**, 181–197.

National Concrete Masonry Association, (2010), *Design Manual for Segmental Retaining Walls*. 3rd Ed., Herndon, Virginia.

PLAXIS. (2005). *Plaxis Finite Element Code for Soil and Rock Analyses*. Version 8.2, P.O. Box 572, 2600 AN Delft, The Netherlands.

Schmertmann, G. R., Chouery-Curtis, V. E., Johnson, R. D., and Bonapart, R. (1987). "Design charts for geogrid-reinforced soil slopes." *Proceedings of Geosynthetics' 87 Conference*, New Orleans, LA, 108–120.

Walters, D. L., Allen, T. M., and Bathurst, R. J. (2002). "Conversion of geosynthetic strain to load using reinforcement stiffness." *Geosynthetics International*, **9**(5-6), 483–523.

Yang, K-H., Zornberg, J. G., Liu, C-N., and Lin, H-D. (2012). "Stress distribution and development within geosynthetic-reinforced soil slope." *Geosynthetics International*, **19**(1), 1–17.

Yang, K-H., Zornberg, J. G., Hung, W-Y., and Lawson, C. R. (2011). "Location of failure plane and design considerations for narrow geosynthetic-reinforced soil wall systems." *Journal of GeoEngineering*, Taiwan Geotechnical Society, April 2011, **6**(1), 13–25.

Yang, K-H., Zornberg, J. G., and Bathurst, R. J. (2010). "Mobilization of reinforcement tensions within geosynthetic-reinforced soil structures." *Earth Retention Conference 3*, *ER2010*, Bellevue, Washington, August 2010, Geotechnical Special Publication, GSP **384**(208), 494–501.

Zornberg, J. G. and Arriaga, F. (2003). "Strain distribution within geosynthetic reinforced slopes." *Journal of Geotechnical and Geoenvironmental Engineering*, ASCE, **131**(2), 141–150.

Zornberg, J. G., Sitar, N., and Mitchell, J. K. (1998). "Limit equilibrium as basis for design of geosynthetic reinforced slopes." *Journal of Geotechnical and Geoenvironmental Engineering*, ASCE, **124**(8), 684–698.